Lata *et al.*
Translational Medicine Communications (2024) 9:20
https://doi.org/10.1186/s41231-024-00176-w

Translational Medicine Communications

RESEARCH Open Access

Abolished clustering of MeCP2^{T158M} can be partially reverted with small molecules

Rodrigo Lata[1], Liesbeth Steegmans[2], Ranie Kellens[2], Marnik Nijs[2], Hugo Klaassen[2], Matthias Versele[2], Frauke Christ[1] and Zeger Debyser[1*]

Abstract

Rett syndrome (OMIM 312750) is a rare neurodevelopmental disorder caused by de novo mutations in the Methyl-CpG Binding Protein 2 (MeCP2) gene located on the X-chromosome, typically affecting girls. Rett syndrome symptoms, characterized by microcephaly and lack of motor coordination, first appear between 6 to 18 months of age. The disease continues to progress until adulthood at which point it reaches a stationary phase. Currently, available therapy for Rett Syndrome is only symptomatic. More than 800 mutations causing Rett syndrome have been described, the most common being T158M (9% prevalence) located in the Methyl-Binding Domain (MBD) of MeCP2. Due to its importance for DNA binding through recognition of methylated CpG, mutations in the MBD have a significant impact on the stability and function of MeCP2. MeCP2 is a nuclear protein and accumulates in liquid–liquid phase condensates visualized as speckles in NIH3T3 cells by microscopy. This speckled pattern is lost with MeCP2 mutations in the MBD such as T158M. We developed a high content phenotypic assay, detecting fluorescent MeCP2 speckles in NIH3T3 cells. The assay allows the identification of small molecules that stabilize MeCP2-T158M and phenotypically rescue speckle formation. To validate the assay, a collection of 3572 drugs was screened, including FDA-approved drugs, compounds in clinical trials and biologically annotated tool compounds. 18 hits showed at least 25% rescue of speckles in the mutant cell line while not affecting wild-type MeCP2 speckles. Primary hits were confirmed in a dose response assay, a thermal shift assay with recombinant MeCP2 and by testing the MeCP2 expression levels. One class of identified hits represents histone deacetylase inhibitors (HDACis) showing 25% speckle rescue of mutant MeCP2 without toxicity. This screening strategy can be expanded to additional compound libraries and will support novel drug discovery.

Keywords MeCP2, Rett Syndrome, HDACi, High content screen

Introduction

Rett syndrome (RTT) is a rare X-linked neurological disorder affecting 1 in 15,000 girls at birth. The disease is caused by *de novo* mutations in the methyl-CpG-binding protein 2 gene (*MECP2)* [1]. RTT patients develop normally during the first months after birth. However, between 6 and 18 months, patients start demonstrating RTT symptoms referred to as the first stage (early onset) [1]. Most patients show hand wringing, delayed motor development and reduced head growth [2, 3]. A partial or complete loss of acquired skills characterizes the second stage (regression). Loss of hand usage and spoken language are the most prevalent symptoms. During this stage, RTT patients may also have difficulties with gait, be unable to walk, and display increased hand wringing or squeezing. Furthermore, respiratory complications, such as hyperventilation and apnea, as well as episodes

*Correspondence:
Zeger Debyser
zeger.debyser@kuleuven.be
[1] Department of Pharmaceutical and Pharmacological Sciences, KU Leuven, Leuven, Flanders, Belgium
[2] Centre for Drug Design and Discovery (CD3) and CISTIM Leuven Vzw, Bio-Incubator 2, Gaston Geenslaan 2, 3001 Heverlee, Belgium

of anxiety emerge during this phase. More than half of RTT individuals develop seizures around 2-3 years of age. This phase has a limited duration, after which individuals with RTT typically transition to the plateau stage, usually between 3 to 5 years of age. Behavioral and cognitive functions tend to stabilize during the plateau phase, and motor skills can degrade at a slower rate [3]. Nevertheless, other medical conditions such as seizures, nutritional problems and other movement disorders may start to manifest [4, 5]. In the last stage, termed late motor deterioration, patients with RTT may experience a further decrease in mobility and display Parkinsonian features, causing severe motor disability [2]. The clinical presentation of RTT varies significantly, and not all patients will undergo each stage or exhibit each clinical feature; the staging system generalizes the typical RTT phenotype.

The severity and progression of the disease are linked to the type of mutation and mosaicism. Thus RTT presents with a wide spectrum of symptoms and severity [1]. Although more than 800 mutations in *MECP2* have been identified in RTT patients [6], 60% of all RTT cases present one of the following eight mutations: R106W, R133C, T158M, R168X, R255X, R270X, R294X or R306C [7]. Recent studies associate the mutation with the symptoms observed in the patients. Based on the mutation present in the patient, it is possible to predict the symptoms and progression of the disease. Among the most common mutations, it is possible to distinguish two groups: R133C, T158M, R294X, and R306C, which cause a less severe RTT phenotype and R106W, R168X, R255X, and R270X, that cause a severe form of RTT [7–12]. This severity is calculated using the clinical features seen in a typical RTT patient, namely hand use, head growth, ability to speak, and respiratory dysfunction [4]. The majority are located in two functional domains: (1) the MBD (85 aa) and (2) the transcriptional repression domain (TRD, 104 aa) [4]. Methyl-CpG Binding Protein 2 (MeCP2) is expressed in two different isoforms, MeCP2E1 and MeCP2E2, which are similar at a structural level, but differ in function and expression patterns. Their role during development is entirely different. MeCP2E1 is expressed at early developmental stages, while MeCP2E2 is only detected in post-natal stages [13]. This indicates that each isoform has an independent role. Moreover, after birth their expression pattern is different. MeCP2E1 has a dynamic expression pattern with lower levels during the day and higher at night, while MeCP2E2 has lower but stable expression levels [14].

MeCP2 is an essential protein in epigenetic regulation and has been identified as a DNA-binding protein, mainly through its MBD. The MBD is the only structured part of the protein, and it is responsible for recognizing the methylation marks in the DNA (Fig. 1A). When associated with DNA, it forms droplets inside the nucleus due to liquid-phase separation. These functional droplets play an important role in MeCP2-chromatin interaction, affecting the condensation of heterochromatin (Fig. 1B) [10, 11]. The MBD of MeCP2 recognizes the CpG-islands in the promoter region of specific genes. The TRD of MeCP2 recruits several binding partners such as Sin3A and histone deacetylases (HDACs), which are responsible for chromatin compaction [15]. RTT-causing mutations located in the MBD impair DNA binding, thus diminishing the recruitment of such binding partners as the HDACs [12]. Together with Sin3A and HDACs, MeCP2 exerts a repressive function in the cell by removing acetyl groups from histones (Fig. 1C) [16]. However, when bound to CREB1, MeCP2 acts as a transcriptional activator (Fig. 1D) [17]. Furthermore, the interaction of MeCP2 with YB1 and LEDGF indicates that MeCP2 is involved in alternative splicing of mRNA (Fig. 1E) [15, 16, 18]. The different binding partners dictate the function of MeCP2, creating many possibilities for corrective approaches.

The most frequent missense mutation, present in approximately 10% of all RTT patients is T158M [4]. Threonine 158 plays an important role in the tandem Asx-Serine Threonine motif of the MBD of MeCP2 and is essential for the binding of MeCP2 to DNA containing 5-methylcytosine (5mC-DNA). The mutant protein shows reduced stability compared to the wild-type contributing to the loss of function [19, 20]. The lower affinity and stability of $MeCP2^{T158M}$ affect the localization of the protein. While the wild-type protein presents normal binding and clustering in NIH3T3 cell lines, this specific mutant presents impaired clustering as previously described [21, 22]. The T158M mutation displays a mild to severe clinical score in most cases yet causes the most severe respiratory problems [23], representing a serious complication in patients leading to frequent respiratory infections. However, it has been shown that overexpressing the mutant form of $MeCP2^{T158M}$ can ameliorate the RTT phenotype in mice, indicating that the protein is still functional [24] and that the loss of stability is the major disease-driving phenotype of the mutant.

Currently, curative treatment for RTT is not available due to the complexity of the disease [25]. Recently the first drug specifically developed for RTT was approved by the FDA [26]. DAYBUE™ reduces brain inflammation by increasing insulin-like growth factor 1 (IGF-1). Due to the monogenetic cause of RTT, gene therapy has been considered as a treatment. Yet, the tight regulation of MeCP2 expression levels and, more importantly,

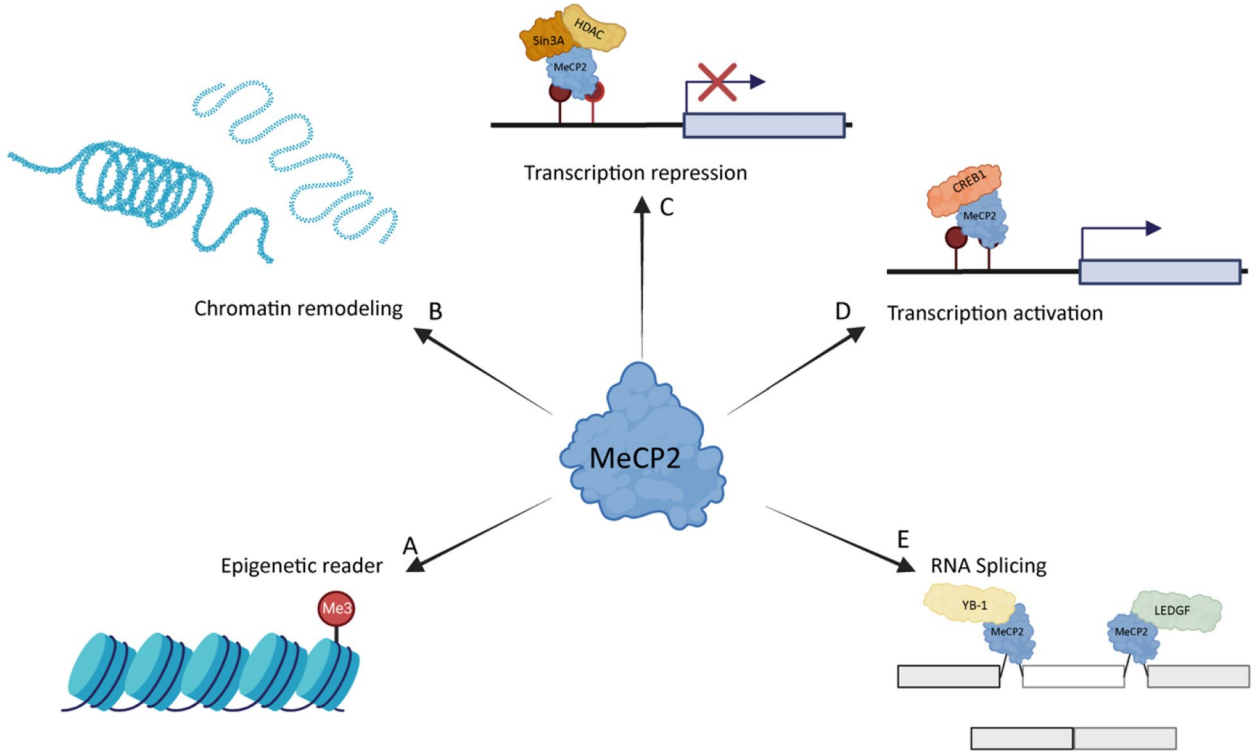

Fig. 1 MeCP2 functions and binding partners **A**) Via its MBD, MeCP2 can recognize methylation marks and act as an epigenetic reader [19, 20]. **B** MeCP2 is able to compact and reorganize the chromatin structure [21, 22]. **C** MeCP2 is involved in transcription regulation when associated with Sin3A and HDACs, the latter of which are repressors [23, 24]. **D** MeCP2 can also act as an activator when bound to CREB1 [17]. **E** The association with YB-1 and LEDGF affects the RNA splicing [15, 16, 18, 25]

the mosaicism of the disease creates a significant challenge for gene therapy approaches.

Here, we established a cell-based phenotypic assay using NIH3T3 cells overexpressing eGFP-tagged MeCP2 or its unstable T158M mutant. The phenotypic difference between both is evident; wild-type MeCP2 is present in pericentromeric speckles in the nucleus while MeCP2^{T158M} is more diffuse because of impaired DNA binding [24]. We used a high-content imaging platform to screen for drugs that can correct MeCP2 binding to DNA. In this model system, we screened small molecules from a repurposing library. More than 3000 compounds were tested, of which 18 hits were considered positive and recovered at least 25% of the number of speckles in the wild-type cell line with a viability of more than 55%. Among the 18 hits, a histone deacetylase inhibitor (HDACi), PCI-34051, was found to restore MeCP2 speckles to 25% at 10 µM. HDACis have previously been tested to treat different neurological disorders such as amyotrophic lateral sclerosis [7], Parkinson's disease and RTT [27, 28]. The identification of HDACis in our phenotypic assay validates our screening platform.

Methods

Cell culture

All cell lines were cultured in a humidified atmosphere of 5% CO_2 at 37°C. They were cultured in Dulbecco's Modified Eagle Medium (DMEM) supplemented with 5% fetal bovine serum (FBS, Gibco) and 0.01% (vol/vol) gentamicin (Gibco) and respective antibiotics for vector selection, 0.005% (vol/vol) blasticidin and 0.001% (vol/vol) puromycin.

Lentiviral vectors and stable cell lines

shRNA targeting MeCP2 was designed using Snapgene and synthesized at Integrated DNA Technologies (IDT, Belgium). The shRNA was generated by annealing the sense and antisense oligos. The annealed product was cloned into the pGAE_SFFV plasmid backbone using the Esp3I restriction enzyme. For MeCP2E1-eGFP, MeCP2E1-eGFPT158M, MeCP2E1-eGFP and MeCP2E2-eGFPT158M back complementation, plasmids were generated using primers (MeCP2_fw GATCTCTAGACCA CCATGGTAGCTGGGATGTTA and MeCP2_rv GGA GGCCTCGAGGTCAGTCTAACTCTCTCGGTCACG GGC) to amplify MeCP2 by PCR and inserted into the

hPGK-eGFP-Puro backbone using XhoI and XbaI restriction enzymes

The viral vector productions were performed as described in. The vector titer was determined by a P24 ELISA test (Fujirebio). NIH3T3 cells stably expressing MeCP2E1-eGFP, MeCP2E1-eGFPT158M, MeCP2E1-eGFP, and MeCP2E2-eGFPT158 M were generated by lentiviral vector transduction and subsequent puromycin (2 µg/mL) selection. Stable polyclonal cells were expanded for further selection of monoclonal cell lines. Two monoclonal lines were selected and verified by fluorescence microscopy for each cell line.

Phenotypic assay

At day 0, 5000 cells from each cell line were plated in a 96-well plate (PhenoPlate 96-well, black, Perkin Elmer) according to the layout in Fig. 3A. The cells were incubated for 24 h in 5% CO_2 and at 37°C. On day 1, 50 µL of compound diluted in cell culture medium was added to each well at a final concentration of 10 µM, compound library provided by CD3. On day 2, the plates were emptied using Bluewasher (Bluecatbio) and the cells were fixed with 4% paraformaldehyde and 5 µg/mL of Hoechst in PBS for 20 min at RT. After fixation PFA was removed and 100 µL of PBS were added. The plates were stored at 4°C. The plates were then imaged using the CX7 (Thermofisher), channel 1- wide-field 386-23: Hoechst 33342, channel 2 – wide-field 488-20: GFP with the 20x objective, with 4 images per well. The images were analyzed using the Cellinsight software (Thermo Fisher). First, the software detects the nucleus of each cell in the Hoechst channel. This is used to quantify the number of cells, whereas the GFP channel detects and quantifies MeCP2 speckles inside the nucleus, which was previously detected by the Hoechst channel. The small molecules were considered positive if they rescued at least 25% of the number of speckles counted in the wild-type condition.

$$Recovery = \frac{(Speckle\ count_{Compound} - Speckle\ count_{negative\ control})}{(Speckle\ count_{positive\ control} - Speckle\ count_{negative\ control})} * 100$$

EC_{50} determination

To calculate the EC_{50} and CC_{50} of each positive hit, the phenotypic assay was performed with a 3-fold serial dilution of each compound starting at 60 µM and 0.6% of DMSO. The half-maximum effective concentration (EC_{50}) was calculated using GraphPad software, a 4-way fitting curve, fixing the top at the maximum recovery observed in the wild-type condition. To calculate the half-maximum cytotoxic concentration (CC50), we considered the total number of cells per well in the non-treated condition as a positive control for viability.

Protein purification

MiniMeCP2 (aa 78 to 309 of MeCP2E2) and miniMeCP2^{T158M} constructs were produced from pET-MeCP2 constructs in E. *coli* BL21. The bacterial culture was grown until an OD_{600} of 0.8in lysogeny broth (LB, Sigma) supplemented with 0.5% glycerol, after which expression was induced using 0.25 mM isopropyl β-D-1-thiogalactopyranoside (IPTG, Sigma-Aldrich) at 18°C for 20 hours. The cells were harvested by centrifugation, 5000 rpm for 15 minutes, and ressuspended in STE buffer (100 mM NaCl (Sigma-Aldrich), 10 mM Tris-HCl (Sigma-Aldrich) pH 7.4 and 0.1 mM ethylenediaminetetraacetic acid (EDTA, (Sigma-Aldrich)) and lysed using lysis buffer (25 mM Tris-HCl, pH 8, 1 M NaCl, 10 µM EDTA, complete protease inhibitor cocktail, 1 mM dithiotreitol (DTT; Sigma-Aldrich)). Then the lysate was sonicated for a minute, 2s on/4s off pulses at 50% amplitude using SFX 250 sonifier (Branson), after sonication 0.1 ug/mL DNAse (Thermofisher Scientific) were added and incubated for 20 minutes on ice. The supernatant was collected after centrifugation for 30 minutes at 15,000 rpm. The fusion protein was captured using His-Select Nickel affinity gel [Sigma-Aldrich);, equilibrated with (wash buffer)and eluted with wash buffer supplemented with 250 mM imidazole (Acros Organics), the eluate was fractioned and spotted on a Whatman paper and stained with Coomassie Brilliant blue G 250 (Merck) dissolved in 50% (v/v) methanol (VWR Chemicals), 10% (v/v) acetic acid (Sigma-Aldrich) and distilled water, to analyze the protein content. The fractions with higher protein content were pooled and concentrated using Amicon filters [Merck] until reaching a volume of 400 µL. The concentrated protein was loaded on a Superose 6 10/300 GL size exclusion column (GE Healthcare), attached to AKTA pure (Cytiva). The column was equilibrated in 50 mM HEPES, 150 mM NaCl and 1 mM DTT. The fractions with absorbance peaks were analyzed on in house SDS-Page followed by a Coomassie stain, the fractions containing mini-MeCP2 and miniMeCP2^{T158M} were pooled and added 10% (v/v) of glycerol and stored at -80°C.

Differential scanning fluorimetry

The melting temperature of miniMeCP2 and miniMeCP2^{T158M} were measured in the CFX Opus 96 Real-time PCR instrument (Bio-Rad, Belgium) using pre-treated (95 °C for 10 min to reduce adherence) PCR tubes and optical flat caps (Bio-rad, Belgium). The final reaction volume was 20 µL (10 µM of miniMeCP2 or 20 µM of miniMeCP2^{T158M}), 10x of SYPRO™ Orange Protein Gel Stain (Thermofisher

Scientific) in DSF buffer (50 mM HEPES and 150 mM NaCl) at room temperature for 20 minutes. After incubation, the sample was heated progressively from 20°C to 95°C (0.2°C steps). Fluorescence measurements were taken at each step from the SYPRO™ Orange dye to generate a melting curve. The T_m of each protein was analyzed using Bio-Rad's CFX Maestro software.

Western blot detection

Cell pellets were obtained from $1x10^6$ HEK293T and NIH3T3 cells and dissolved in 100 µL of RIPA buffer (Thermofisher Scientific), followed by an incubation of 30 minutes on ice. The supernatant was collected after 10 minutes of centrifugation at 17000 g at 4 °C. Protein concentration was measured by the bicinchoninic acid (BCA) assay (Thermofisher Scientific). A total of 30 µg of protein extract was loaded on a 4%-15% criterion TGX pre-cast Midi gel (Bio-Rad) gel and run for 1 hour at 130 V in Tris-glycine buffer (Bio-rad). The proteins were transferred onto a nitrocellulose membrane (Amersham) using the transblot SD Semi-dry transfer cell (Bio-rad) using the Turbo blotting protocol from the manufacturer. The membrane was incubated for 1 h at room temperature with 4% of skimmed milk in PBS-T (PBS with 0.1% TrintonX-100). After being washed 3 times with PBS-T, the membrane was incubated overnight at 4°C with primary antibodies, 1/500 dilution of rabbit anti-MeCP2 (Cell signaling), 1/1000 chicken anti-GFP and 1/10000 dilution of mouse anti-vinculin (Sigma Aldrich). After the incubation with the primary antibody, the membrane was washed with PBS-T and incubated with the secondary antibodies for 1 hour at room temperature. The secondary horseradish peroxidase (HRP)-conjugated antibodies used were goat anti-rabbit, Goat anti-chicken and goat anti-mouse, diluted 1:5000 in blocking buffer. The secondary antibody was washed away with PBS-T, and stained proteins were detected by chemiluminescence (Clarity Western ECL, Bio-rad). The western blot signal was acquired using Amersham Image Quant8000 (GE Healthcare), and the figures were analyzed using ImageLab (BioRad).

Immunocytochemistry

The cells were seeded in an 8-well chamber slide (Ibidi), with 25000 cells for NIH3T3 and 40000 cells for HEK293T. After attaching, cells were fixed in 4% (v/v) paraformaldehyde (PFA) (Sigma-Aldrich) for 20 minutes at room temperature and washed three times with PBS (Thermofisher Scientific). Cells were permeabilized using 0.1% (v/v) tritonX-100 (Acros organics) in PBS, followed by 30min incubation with blocking buffer, 0.5% BSA and 0.1% Tween-20 (AppliChem) at room temperature. The primary antibodies, 1/500 rabbit anti-MeCP2 (Cell Signaling) and 1/500 mouse anti-Flag M2 F1804 (Sigma-Aldrich), were incubated overnight at 4°C. The secondary antibodies, donkey anti-rabbit Alexa fluor 488, donkey anti-mouse Alexa fluor 633, and Hoechst 33342, were added to each well after washing the primary antibody 3 times with a blocking buffer. The secondary antibodies were incubated for 1 h at room temperature, and three additional washing steps were performed before storing the samples at 4°C. Immunocytochemistry (ICC) images were acquired using a confocal imaging microscope (Zeiss LSM 880) and analyzed using ZenBlack from Zeiss.

Results

Construction of monoclonal cell lines overexpressing MeCP2E1-eGFP or MeCP2E1-eGFP^{T158M}

The differential phenotype of MeCP2 and MeCP2^{T158M} has been studied in murine NIH3T3 [12, 13]. Wild-type MeCP2 forms clear pericentromeric speckles, while MeCP2^{T158M} displays fewer speckles due to impaired affinity to chromatin [12]. Speckles are known to represent liquid phase condensates [12]. To identify compounds targeting human MeCP2, we initially aimed to detect if, in human cell lines such as HEK293T, a different phenotype between wild-type and mutant MeCP2 could be visualized. Unfortunately, no speckled pattern was present in HEK293T, and the difference between the wild-type and MeCP2^{T158M} was not easily spotted in this cell line. Instead, we depleted endogenous mouse MeCP2 by shRNA knock down and overexpressed the human isoform C-terminally tagged with eGFP in murine NIH3T3 cells (Fig. 2). We generated isoform-specific cell lines to compare MeCP2E1 with MeCP2E2. In Fig. 2 human MeCP2E1-EGFP adopts the typical speckled pattern of endogenous mouse MeCP2. Moreover, the difference between MeCP2 and MeCP2^{T158M} speckles was clear for both isoforms, indicating that the eGFP-tag does not affect the binding of MeCP2 to DNA. This difference encouraged us to establish a phenotypic assay.

The phenotypic assay accurately assesses the speckled pattern of wild-type MeCP2E1 and MeCP2E1^{T158M}. MeCP2E1 forms distinct and clear pericentromeric speckles in the nucleus, whereas MeCP2E1^{T158M} is distributed dispersedly (Fig. 2). Stable NIH3T3 cell lines expressing MeCP2E1-eGFP or MeCP2E1-eGFP^{T158M} were generated using lentiviral vector transduction and puromycin-based selection, followed by clone selection to avoid heterogeneous expression levels. Confirmation of the phenotype was achieved through fluorescence microscopy and quantification of speckles per nucleus, which revealed an average of 13.6 ± 0.6 speckles per cell for MeCP2E1eGFP and only 1 ± 0.5 speckle for MeCP2E1-eGFP^{T158M} (Fig. 3D).

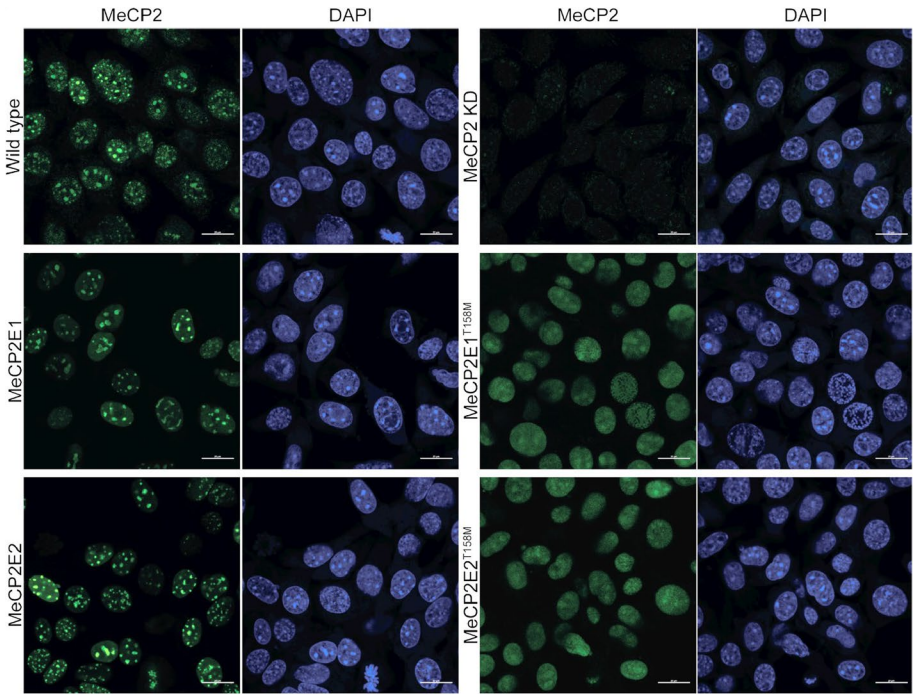

Fig. 2 MeCP2 phenotype in various cell lines. Confocal microscopy images show the cellular distribution of MeCP2 in NIH3T3 wild–type, and MeCP2 knockdown (KD) cells. NIH3T3 cells overexpressing MeCP2E1-GFP, MeCP2E1-T158M-eGFP, MeCP2E2-eGFP or MeCP2E2-T158MeGFP display different distributions of MeCP2. The cell lines overexpressing MeCP2-eGFP are monoclonal cell lines. Endogenous MeCP2 was detected with rabbit anti-MeCP2 antibody (1:500) and anti-rabbit Alexa 488 secondary antibodies (1:1000) (upper row). In contrast, eGFP-tagged MeCP2 was detected in the 488 nm channel in green (first column) and DAPI in the 405 nm channel (blue).Images acquired with Zeiss LSM880 and analyzed with ZenBlack software Scale bar – 20 µm

As a positive control in the screen, NIH3T3-MeCP2E1-eGFP cells were seeded in wells A1 to D1 and E12 to H12, while the negative control NIH3T3-MeCP2E1-eGFP^{T158M} cells were seeded in wells E1 to H1 and A12 to D12. Furthermore, all wells were treated with DMSO to a final concentration of 0.1% to account for the solvent in the compounds that were diluted. The remaining wells of each plate were filled with NIH3T3-MeCP2E1eGFP^{T158M}, and the small molecules were added at a final concentration of 10 µM.

We screened 3572 small molecules from a Drug-Repurposing Library of the Centre for Drug Design and Discovery (CD3, Leuven) to assess their ability to correct MeCP2^{T158M} binding to DNA and facilitate the formation of pericentromeric domains. To ensure reliable results, controls were placed on the outer wells of the plate, and the Z'-factor was calculated using mean values and standard deviation of speckles per cell in NIH3T3-MeCP2E1-eGFP and NIH3T3-MeCP2E1-eGFP^{T158M} (Fig. 3C). The assay demonstrated a robustness with an average Z'-prime score of 0.7 ± 0.1. Small molecules were considered positive hits only if they showed at least 25% recovery of the wild-type speckle count with over 55% cellular viability. Of the 3572 small molecules, 118 showed at least 25% rescue of the phenotype, but only 28 passed toxicity criteria. To ensure validity, individual inspection of images led to the removal of 10 compounds from the selection due to saturation in the GFP channel. In the final list of 18 compounds, the range of rescue varied from 25.7% up to 36.6%, with cell viability ranging from 55.5% to 99.2% (Table 1).

Compounds demonstrate a dose–response activity rescuing MeCP2 expression

To validate the positive hits from the high content screen, we determined their dose response using a ten-step 3-fold serial dilution of each compound, starting at 60 µM. In parallel, we included four HDACis detailed in Table 2, which were initially classified as negative in the high content screen. The objective was to comprehend whether HDACis impact MeCP2's DNA binding affinity, despite their lack of positive effects in the initial screening. In the first screening, several compounds demonstrated activity. However, Tubastatin-A (TBA) did not reach the required 25% threshold and additionally demonstrated toxicity. Mocetinostat displayed activity

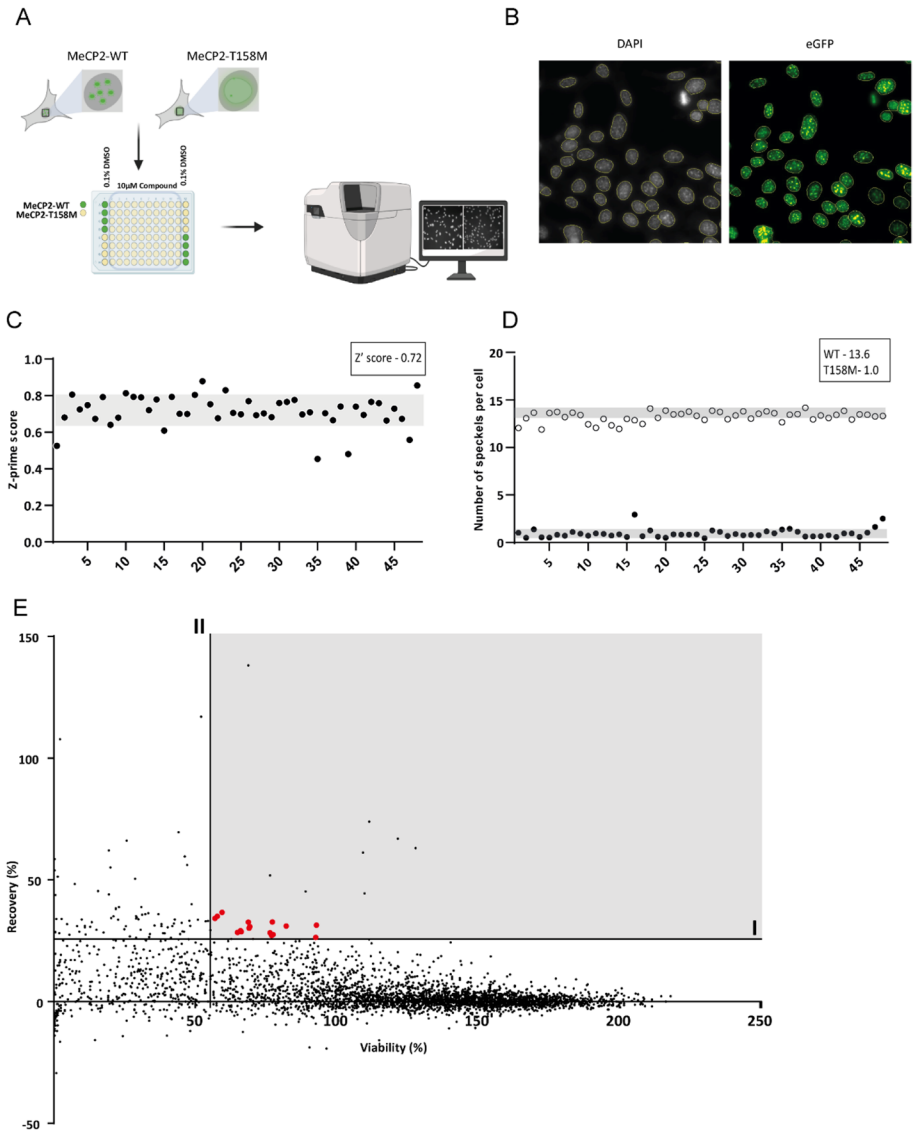

Fig. 3 High content screen. **A** Schematic representation of the high content screen pipeline. The cell lines NIH3T3-MeCP2E1-eGFP and NIH3T3-MeCP2E1-eGFP^{T158M} were seeded in 96-well plates, the wells with wild-type MeCP2 are displayed in green, those with MeCP2^{T158M} in yellow. **B** Representative picture of DAPI staining and delimitation of nucleus (yellow line). Representation of eGFP detection in the nucleus and respective spot detection (yellow dots). **C** Individual representation of the Z'-score of each plate. The average Z'-score of the screen was 0.72 ± 0.08. **D** Number of speckles detected in the wild-type control (positive control) and the T158M cell line (negative control) per plate. **E** Representation of the individual values for each compound for Viability (%) X axis and recovery (%). Horizontal line (I) – Compounds that recover more than 25% of the wild-type phenotype. Vertical line (II) – Compounds that show 25% recovery and at least 55% viability. The grey area represents the compounds considered as positive hits. Red dots represent the 18 compounds considered as positive hits

but was associated with toxicity. Entinostat showed a recovery below the 25% threshold, yet it did not exhibit any toxicity allowing us to increase the concentration during dose response. Despite MC-1568 meeting both thresholds, it was initially excluded due to its autofluorescence. However, it was included in the dose-response to explore the possibility of reduced autofluorescence at lower concentrations without compromising efficacy. This decision turned out to be correct as we observed an increase in the number of speckles at very low concentrations, indicating a positive effect at reduced autofluorescence levels.

Table 1 List of positive hits in high content screening. Rescue represents the number of speckles in % relative to wild-type. Viability in % relative to a DMSO control

Compound	Class	Rescue (%)	Viabilty (%)
Compound 1	Kinase inhibitor	36.6	59.5
Compound 2	Anti-arrhythmic	35.0	57.8
Compound 3	Disinfectant	34.1	57.0
Compound 4	Muscle relaxant	32.7	77.3
Compound 5	Kinase inhibitor	32.6	68.8
Compound 6	Anti-bacterial	31.4	92.9
Compound 7	Muscle relaxant	31.0	82.2
Compound 8	Anti-malaria	30.8	69.3
Compound 9	Topoisomerase inhibitor	30.1	69.0
Compound 10	Kinase inhibitor	29.3	55.3
Compound 11	Kinase inhibitor	29.1	66.0
Compound 12	Anti-fungal	28.7	66.3
Compound 13	Anti-inflammatory	28.4	64.9
Compound 14	Anti-histaminic	28.2	76.4
Compound 15	Muscle relaxant	27.5	77.5
Compound 16	Glucocorticoid	27.1	77.0
Compound 17	Corticosteroid	25.7	70.4
PCI-34051	HDAC 8	25.7	62.7

Table 2 List of HDACis included in the dose response (DR) assay and corresponding structures

Compound	Target	Rescue (%)	Viability (%)	Structure
PCI-34051	HDAC8 [26]	25.7	62.7	a
MC-1568	HD1, HDAC4 5 [29]	45.2	89.0	b
Tubastatin-A HCL	HDAC6 [30]	19.8	29.3	c
Mocetinostat	HDAC1, 2 and 3 [27]	30.9	41.9	d
Entinostat	HDAC1 and 3 [28]	13.5	98.4	e

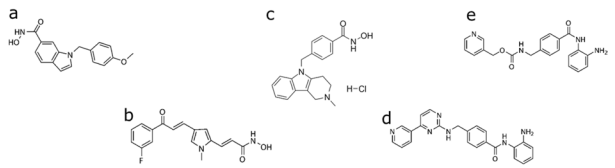

Considering that MeCP2 has two isoforms with different expression patterns and functions [8], we also included MeCP2E1 and E2 in the dose-response assay to evaluate if the compounds have similar effects on both isoforms.

As described in Table 3, for most compounds, a dose-response (EC_{50}) could be determined. Despite showing a dose-response, the maximum recovery observed was 6 speckles per cell, corresponding to less than 50% of the wild-type. Thus, we calculated the EC50 taking that number as the maximum recovery possible. The EC_{50} of the positive hits for MeCP2E1^{T158M} ranged from 0.6 to 113.78 µM. For the specific class of the HDACis, there was less variability, with a range from 6.09 µM to 14.67 µM. The IC_{50} of entinostat, on the contrary, was only 113.78 µM, but it shows high variability (Table 3). For MeCP2E2^{T158M} similar results were obtained, the EC_{50} for each compound was in the same range as with MeCP2E1^{T158M} (Supplementary Table 1). The toxicity levels were consistent across all cell lines tested. However, the selectivity index is low, indicating that activity is associated with toxicity.

The hits from the phenotypic screen were subjected to a differential scanning fluorimetry (DSF) assay to investigate their impact on the melting curve of miniMeCP2^{T158M}. We purified a truncated version of MeCP2, named mini-MeCP2, which includes MBD, ID, and TRD (Fig. 4A). Notably, the wild-type mini-MeCP2 exhibited a melting temperature (Tm) of 45°C, while the mutant mini-MeCP2^{T158M} displayed a significantly reduced Tm of 32.5°C (Fig. 4B), indicating decreased protein stability for the mutant MeCP2. Using this assay, we assessed the effect of the hits from the phenotypic screening. Among the 15 compounds tested, only compound 13 exhibited a significant increase in the melting temperature, indicating its direct binding to mini-MeCP2^{T158M}. In contrast, the HDACis that target class I HDAC, Entinostat, and Mocetinostat, showed a significant decrease in the melting temperature of miniMeCP2^{T158M} when tested against wild-type mini-MeCP2. Neither compound 13 nor HDACis displayed a significant effect on the wild-type protein, indicating that compound 13 specifically targets the mutant protein.

HDACis affect MeCP2 expression

Considering that the HDACis did not increase the melting temperature of MeCP2^{T158M}, we anticipated that they might influence its expression levels. To investigate this, we treated HEK293T and NIH3T3 wild-type cells with 10 µM of each HDACi. By comparing both cell lines, one with mouse MeCP2 and the other with human MeCP2, we aimed to test the impact of HDACis in cells expressing both isoforms of the respective MeCP2 variants. Since different HDACis target various HDAC classes, this allowed us to explore the effects of individual HDACs on the expression of MeCP2. As shown in Fig. 5, treatment with HDACis reduced MeCP2 levels, as reported before [28]. Treatment with Tubastin-A, Mocetinostat, or Entinostat reduces MeCP2 levels in both cell lines. In contrast, MC-1568 shows a reduction of MeCP2 levels

Table 3 EC_{50} and CC_{50} values (μM) in dose response assay for NIH3T3-MeCP2E1 and NIH3T3-MeCP2E1^{T158M}. NIH3T3-MeCP2E1 $n=2$, NIH3T3-MeCP2E1^{T158M} $n=3$. Compounds 6,11,16 were not available for retesting (N/A)

	E1^{T158M}					E1	
	EC_{50}		CC_{50}		Selectivity index	CC_{50}	
	Average	StDev	Average	StDev		Average	StDev
Compound 1	1.80	1.63	1.84	0.91	1.02	2.59	2.14
Compound 2	8.22	7.55	8.66	5.55	1.05	9.81	6.46
Compound 3	13.23	5.76	14.85	6.55	1.12	9.02	3.47
Compound 4	5.57	2.13	6.84	3.07	1.23	5.80	4.21
Compound 5	3.46	1.29	0.83	0.37	0.24	0.61	0.34
Compound 6	N/A	N/A	N/A	N/A	N/A	N/A	N/A
Compound 7	15.78	11.87	12.14	0.75	0.77	12.44	8.83
Compound 18	51.13	38.27	36.82	12.46	0.72	29.31	0.00
Compound 19	0.60	0.81	2.34	2.06	3.92	4.00	2.18
Compound 10	4.47	3.78	4.39	2.39	0.98	5.49	4.40
Compound 11	N/A	N/A	N/A	N/A	N/A	N/A	N/A
Compound 12	6.41	4.31	6.93	0.97	1.08	6.52	4.75
Compound 13	6.79	1.64	7.52	1.86	1.11	5.74	2.69
Compound 14	13.67	5.19	8.73	0.72	0.64	8.56	6.04
Compound 15	2.85	1.76	2.18	1.01	0.76	3.48	2.85
Compound 16	N/A	N/A	N/A	N/A	N/A	N/A	N/A
Compound 17	15.50	13.35	5.85	3.72	0.38	28.20	0.00
Mocetinostat	8.47	0.55	3.89	0.33	0.46	3.59	1.99
Entinostat	113.78	92.66	35.29	7.66	0.31	16.94	10.38
PCI-34051	14.67	10.15	16.97	5.36	1.16	11.71	2.94
Tubastatin-A	7.45	4.64	2.53	0.52	0.34	3.44	0.97
MC-1568	6.09	1.28	11.20	1.71	1.84	13.54	6.41

in the NIH3T3 cell line but no effect in HEK293T cells, whereas PCI-34051 shows an impact in HEK293T but not in NIH3T3, indicating distinct mechanisms in these cell lines.

Impact of hits on MeCP2 expression

To investigate the effect of the compounds on the expression of MeCP2, we tested their impact on the endogenous MeCP2 expression levels in HEK293T and NIH3T3 cells since most hits did not directly affect miniMeCP2^{T158M}. We incubated each cell line for 24 hours with 10 μM of each compound to replicate the conditions used in the phenotypic assay. Our results showed that compounds 9 and 4 increased the expression levels of MeCP2 in NIH3T3 cells by roughly 2-fold compared to the DMSO control. On the other hand, compounds 15 and 17 decreased the expression levels of MeCP2 by less than 1.5-fold. In HEK293T cells, we observed a significant increase in the expression levels of MeCP2 with the addition of compound 9. Compound 4 also increased the protein levels of MeCP2 in HEK293T cells, although not to the same extent as compound 9. While the remaining compounds did not show a statistically significant increase in MeCP2 expression, we did observe a slight overexpression. Therefore, these results indicate that the observations made in mouse cell lines NIH3T3 can be partially translated to human cell lines (Fig. 6).

Discussion

Finding a specific treatment for RTT is a high unmet medical need and has been the aim of many research groups in academia and industry in recent years. Despite the significant effort and advances, there is still no curative therapy focused on correcting the impact of RTT mutations on the function of MeCP2. Recently, the FDA approved the first specific treatment for RTT patients, trofinetide, an analog of insulin-like growth factor 1 (IGF-1), acting as an anti-inflammatory agent [26]. Although it is considered a specific RTT treatment, trofinetide does not target MeCP2, the cause of RTT. Other clinical trials are ongoing to deliver a functional version of MeCP2 using adeno-associated viral vectors (AAV) [31]. The

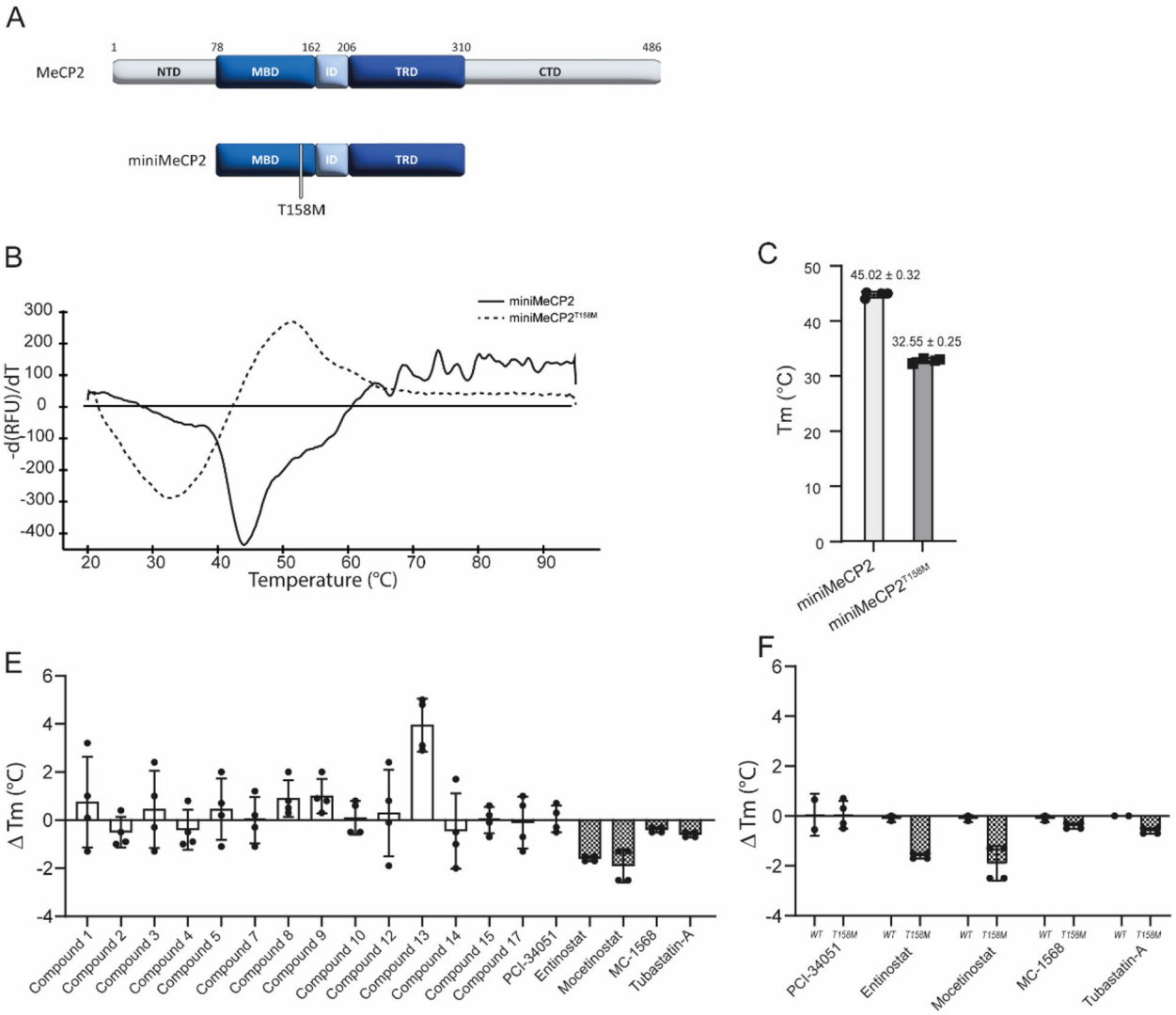

Fig. 4 The protein stability of miniMeCP2^{T158M} is affected by compound 13. **A** Schematic representation of full-length MeCP2 and miniMeCP2. **B** Melting curve of miniMeCP2 and miniMeCP2^{T158M} in DSF assay, negative peak of fluorescence represented. **C** Melting temperature (Tm °C) of miniMeCP2 and miniMeCP2^{T158M}, calculated from the melting cure in the DSF assay. **D** Graphical representation of the thermal shift of miniMeCP2.^{T158M} when incubated with 10 µM of compound relative to DMSO control. $n=4$. **E**) Effect of 10 µM of the five different HDACis in miniMeCP2 wild-type and T158M. $n=2$

gene therapy approach seems to face many obstacles due to the mosaicism of RTT, specifically the targeting of the unhealthy cells and delivery of the correct dose to avoid MeCP2 duplication syndrome (MDS) [32]. RTT is caused by more than 800 different mutations in MeCP2, leading to pleiotropic effects, such as malfunction, reduced expression, or expression of non-functional truncated MeCP2 proteins. Due to these pleiotropic effects, finding a single drug to cure RTT will be a difficult, if not impossible, endeavor. Here, we focused on the most common single point mutation, T158M, accounting for almost 10% of all RTT patients [16].

Lamonica *et al.* [24] showed that overexpression of MeCP2^{T158M} in mice rescues the RTT phenotype, indicating that the protein retains its affinity for DNA yet cannot exert this function sufficiently due to reduced stability, which other authors have also suggested [20, 33]. We established a phenotypic screen to identify small molecules that can revert this phenotype and allow MeCP2^{T158M} to form pericentromeric domains as the wild-type does. The crucial part of this work was to create a cell model in which the pericentromeric domain formation of MeCP2 and MeCP2^{T158M} could be discriminated. Initially, we tried to establish the assay in human

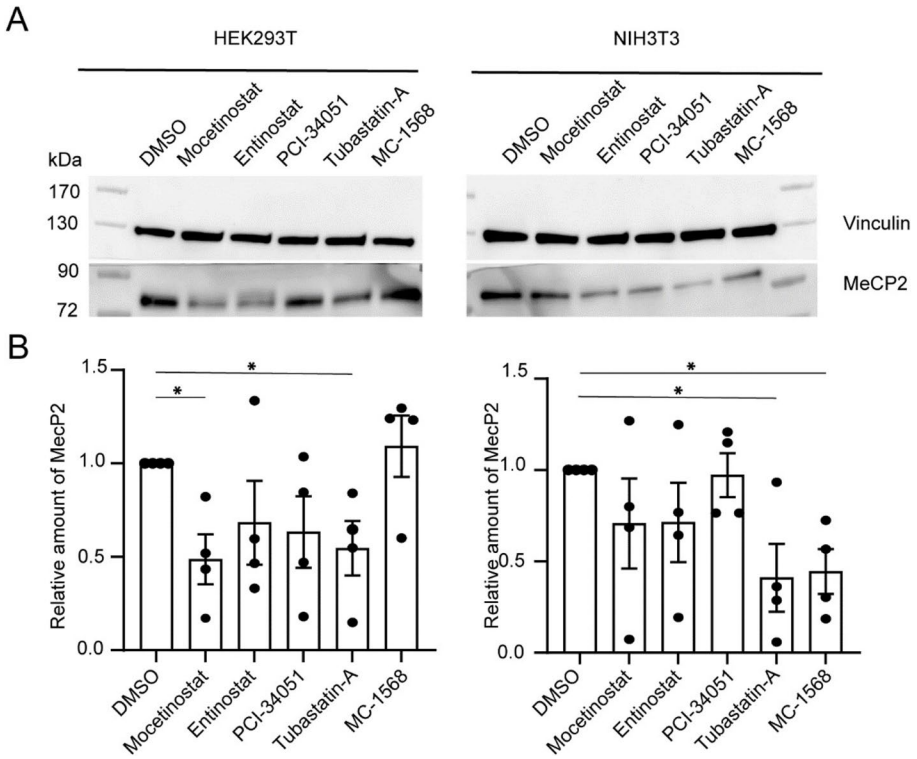

Fig. 5 HDAC inhibitors affect MeCP2 protein levels. **A** Representative blots of the effect of 10 µM of HDACi during 24 h on MeCP2 levels in HEK293T (left) or NIH3T3 (right). **B** Densitometry measurements of MeCP2 levels, normalized to the DMSO control. Data was represented as mean ± SEM of 4 experiments (each dot). Mann–Whitney test was used to assess statistical differences. * *p* value < 0.05

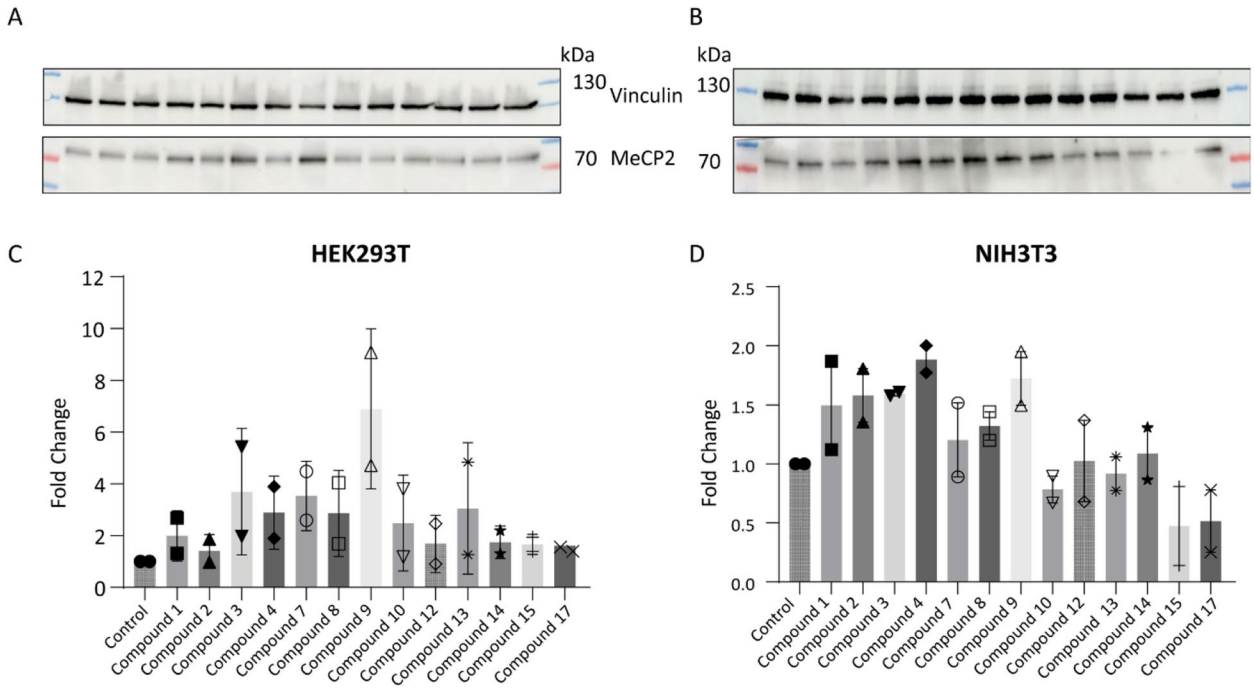

Fig. 6 Effect of hit compounds on MeCP2 Expression **A**, **B**) Detection of the endogenous level of MeCP2 HEK293T and NIH3T3 cells after 24 h incubation with 10 µM of each positive hit from the high content screen. Vinculin was used as the loading control. **C**, **D** Bar graphs represent quantification by densitometry of MeCP2 relative to vinculin in two independent experiments

cell lines; however, the difference observed between MeCP2 and MeCP2^{T158M}in human cell lines was less clear than in mouse cell lines since the speckled pattern is mouse-specific, as described earlier [13]. The speckled pattern displayed by mouse cells is associated with heterochromatin arrangement independently from MeCP2 [13]. Despite the high conservation of human and mouse MeCP2, we engineered NIH3T3 cells (mouse fibroblasts) to express human MeCP2 to ensure that the identified drugs act on the human protein.

In the phenotypic assay, the number of MeCP2 speckles in the nucleus of NIH3T3 cells was quantified. MeCP2^{T158M} was classified as having abolished clustering, meaning it still binds to DNA but does not form the clear speckled pattern [12, 21]. To reduce the individual experimental steps in the screening process, minimizing variability and the duration of the assay, we opted to tag human MeCP2 with eGFP. We explored both N-terminal and C-terminal eGFP tags, and there was no difference in the speckle formation. However, since MeCP2E1 and MeCP2E2 differ only in the N-terminal domain that determines protein stability by the N-end rule, we decided to continue with the C-terminal tag to avoid masking the difference between the two isoforms. To identify compounds rescuing the MeCP2 function, a repurposing library with compounds from different chemical classes was screened. From the 3572 compounds, 18 hits were identified. To consider a compound as a hit, a rescue of at least 25% of the number of speckles observed in the wild-type was required. Therefore, around 0.5% of compounds were positive, which is in line with other similar screening assays [34]. This provided strong proof of concept that our screening strategy allows us to identify hits modifying the phenotype observed in NIH3T3 cells. The hits identified rescued a maximum of 36% of the wild type phenotype, indicating that the abolished clustering of MeCP2^{T158M} can only be partially rescued.

Interestingly, the compounds considered positive belong to very different classes, including kinase inhibitors, muscle relaxants and HDACis (Table 1), reflecting the diverse nature of our repurposing library and suggesting that correcting MeCP2^{T158M} abolished clustering can be achieved via multiple pathways including direct binding to MeCP2^{T158M} [21].

In our assay, we compared both MeCP2 isoforms carrying the T158M mutation. When we tested the positive hits and the additional HDACis in the dose response assay we could show that all compounds display a dose response curve demonstrating the specificity of the compounds. The EC_{50} value was generally lower for MeCP2E2^{T158M}, which can be explained by the higher affinity of MeCP2E2 for DNA that can be increased with chaperone-like molecules or post-translational modification of MeCP2 [5, 35].

Our main goal was to find chaperone-like small molecules that stabilize MeCP2^{T158M}. Hence, we investigated whether the compounds affect the folding of the protein. We decided to use mini-MeCP2, which only contains MBD, ID, and TRD, avoiding the differences between isoforms. As expected, the wild-type miniMeCP2 showed a higher melting temperature than the less stable MeCP2^{T158M}. The difference of 13°C creates a window to measure compounds that restore the melting temperature of miniMeCP2^{T158M}. Interestingly, compound 13 increased the melting temperature of miniMeCP2^{T158M} by 5°C, implying only this compound directly binds to MeCP2. Although it was not possible to test if the increase of the melting temperature would translate into higher stability of miniMeCP2^{T158M}, the results from compound 13 show that the rescue of MeCP2^{T158M} can be achieved directly or indirectly, opening the door for structural activity research of compound 13.

Additionally, we explored the effect of compound 13 and the remaining hits from the HTS on the expression levels of MeCP2 to understand if the effect observed was due to overexpression of the mutant protein. As shown in the results section, compounds 4 and 9 significantly increased the expression levels of endogenous MeCP2, indicating that these compounds indirectly affect the availability of MeCP2 in the cell. However, it is important to reiterate that overexpression of MeCP2 can lead to MDS and is thus not ideal for RTT patients. Nevertheless, this finding gives an insight into the structure of MeCP2 and how a controlled overexpression of MeCP2^{T158M} can be a therapeutic approach.

By screening the repurposing library, HDACis were identified as one promising class of compounds. This is in line with previous reports. Trichostatin and TBA, tested in Mecp2 knockout and MeCP2$^{308/Y}$, respectively, showed improvement in the phenotype. While HDACis are known to regulate gene expression, we observed that compound 13, Mocetinostat and Entinostat affected the melting temperature of miniMeCP2^{T158M} suggesting that they also have a direct effect on MeCP2. Previous studies with the generic HDACi Trichostatin, have shown that HDACis hyperacetylate histones in non-neuronal cells and decrease the levels of MeCP2 [28]. Although this seems paradoxical to what we are pursuing, the chromatin binding affinity is significantly increased due to a decrease in the phosphorylation of MeCP2-S164 [28], which can explain the increase in the number of speckles detected in MeCP2^{T158M} cell lines. Our results show that TBA reduces MeCP2 levels as described for Trichostatin. However, it is worth noting that while

Trichostatin is a generic HDACi, TBA specifically targets HDAC6, a class IIb HDAC. TBA has been tested in the context of RTT: treatment of MeCP2$^{308/y}$mice significantly improved the mouse's behavior and survival. TBA increases α-tubulin acetylation, promoting axonal trafficking by increasing microtubule stability [16]. In MeCP2 knockout neurons, BDNF trafficking is deficient but can be restored with TBA [16]. The effect of TBA in MeCP2$^{308/y}$ mice suggests that HDACis could be used to treat RTT. Our results show that HDACis increase the affinity of MeCP2 for DNA as previously described and the mechanism of action of TBA is very similar in both human and mouse cell lines. Unfortunately, it was impossible to test the phosphorylation levels of S164 because the antibody used in previous reports is not commercially available.

The other HDACis tested target Class I HDACs (HDAC1, 2 and 3) and HDAC8 that are evolutionarily related [36, 37]. The HDAC1, 2 and 3 inhibitors, Mocetinostat and Entinostat, showed similar effects in both MeCP2 isoforms. HDAC1 and 2 form a complex with Sin3A [38], while HDAC3 is recruited by the N-CoR/SMRT corepressor complex that binds MeCP2. MeCP2 has been described as interacting indirectly with HDACs using Sin3A as a bridging element. This complex increases the deacetylation of the chromatin, repressing gene transcription [39].

On the other hand, the results from PCI-34051, the HDAC8 inhibitor, are more complex to interpret. PCI-34051 has an IC_{50} of 10 nM, 1000 fold lower than the concentration used in our experiment. At such a high concentration, PCI-34051 also affects HDAC1 and HDAC6 in HEK293T, showing a similar effect as TBA. Therefore, the effect seen may not specifically be due to the inhibition of HDAC8.

HDACis can improve the RTT phenotype in mouse models as shown in previous studies [27, 28], However, in our assay, the selectivity index is very narrow, which is consistent with the pleiotropic effects of HDACi, thus treating RTT with HDACis may not be realistic since HDACs are involved in many different pathways. Currently HDACis are used to treat different cancers such as lymphoma or myeloma or neurological disorders such as epilepsy or bipolar disorders [40].

In conclusion, we established and validated a screening platform to identify compounds that rescue speckle formation in MeCP2^{T158M} NIH3T3 cells. This platform is amenable to screening large chemical libraries and can be expanded to test other mutations that show abolished clustering of MeCP2, namely R106W and R133C, increasing the type and number of patients that can be reached. Apart from drug discovery for RTT, hits may help to understand how different cellular pathways affect MeCP2 and MeCP2 mutants.

Abbreviations

aa	Amino acid
AAV	Adeno associated viruses
BCA	Bicinchoninic acid
BDNF	Brain-derived neurotrophic factor
CC_{50}	Cytotoxic concentration
CTD	C-terminal domain
DSF	Differential Scanning fluorimetry
EC_{50}	Effective concentration
FRAP	Fluorescence recovery after photobleaching
HDAC	Histone deacetylase
hPGK	Human phosphoglycerate kinase
HTS	High throughput screening
ICC	Immunocytochemistry
IGF-1	Insulin like growth factor 1
iPSC	Induced pluripotent stem cell
KD	Knockdown
MBD	Methyl binding Domain
MDS	MeCP2 duplication
MeCP2	Methyl CpG binding Protein 2
Ncor	Nuclear Receptor corepressor
NTD	N-terminal domain
RTT	Rett Syndrome
sgRNA	Single guide RNA
Tm	Melting temperature
TRD	Transcription repression domain
WT	Wild type

Supplementary Information

The online version contains supplementary material available at https://doi.org/10.1186/s41231-024-00176-w.

Supplementary Material 1.

Supplementary Material 2.

Acknowledgements
I acknowledge Siska Van Belle, Paulien van de Velde, Saskia Lesire and Yannick Hoogvliets for excellent technical assistance.

Authors' contributions
Conception and design, Zeger Debyser and Frauke Christ. Material preparation and data collection Rodrigo Lata, Marnik Nijs, Liesbeth Steegmans and Rannie Kellens. Data analysis Rodrigo Lata, Marnik Nijs, Hugo Klaassen and Matthias Versele. Writing original draft, Rodrigo Lata, Zeger Debyser. All authors read and approved the final manuscript.

Funding
Financial support was received from Celsa (KU Leuven) CELSA5439-DOA/18/003 and FWO (EFH-D7808-G0C2620N FWO).

Availability of data and materials
The datasets generated during the current study are not publicly available due to intellectual property protection but are available from the corresponding author on reasonable request.

Declarations

Ethics approval and consent to participate
Not applicable.

Consent for publication
Not applicable.

Competing interests
The authors have no relevant financial or non-financial interests to disclose.

Received: 23 December 2023 Accepted: 22 May 2024
Published online: 05 June 2024

References

1. Amir RE, et al. Rett syndrome is caused by mutations in X-linked MECP2, encoding methyl-CpG-binding protein 2. Nat Genet. 1999;23:185–8.
2. Pejhan S, Rastegar M. Role of DNA Methyl-CpG-binding protein MeCP2 in rett syndrome pathobiology and mechanism of disease. Biomolecules. 2021;11:75.
3. Neul JL, et al. Rett syndrome: revised diagnostic criteria and nomenclature. Ann Neurol. 2010;68:944–50.
4. Krishnaraj R, Ho G, Christodoulou J. RettBASE: Rett syndrome database update. Hum Mutat. 2017;38:922–31.
5. De MartínezPaz A, et al. MeCP2-E1 isoform is a dynamically expressed, weakly DNA-bound protein with different protein and DNA interactions compared to MeCP2E2. Epigenetics Chromatin. 2019;12:63.
6. Ghosh RP, Horowitz-Scherer RA, Nikitina T, Shlyakhtenko LS, Woodcock CL. MeCP2 binds cooperatively to its substrate and competes with histone H1 for chromatin binding sites. Mol Cell Biol. 2010;30:4656–70.
7. Hite KC, Kalashnikova AA, Hansen JC. Coil-to-helix transitions in intrinsically disordered methyl CpG binding protein 2 and its isolated domains. Protein Sci. 2012;21:531–8.
8. Olson CO, Zachariah RM, Ezeonwuka CD, Liyanage VRB, Rastegar M. Brain region-specific expression of MeCP2 isoforms correlates with DNA methylation within Mecp2 regulatory elements. PLoS One. 2014;9:e90645–e90645.
9. de MartínezPaz A, et al. Circadian cycle-dependent MeCP2 and brain chromatin changes. PLoS One. 2015;10:e0123693.
10. Zhang H, Qin W, Romero H, Leonhardt H & Cardoso MC. Heterochromatin organization and phase separation. Nucleus. 2023;14. Preprint at https://doi.org/10.1080/19491034.2022.2159142.
11. Kudo S, et al. Heterogeneity in residual function of MeCP2 carrying missense mutations in the methyl CpG binding domain. J Med Genet. 2003;40:487.
12. Wang L, et al. Rett syndrome-causing mutations compromise MeCP2-mediated liquid–liquid phase separation of chromatin. Cell Res. 2020;30:393–407.
13. Pantier R, et al. MeCP2 binds to methylated DNA independently of phase separation and heterochromatin organisation—bioRxiv. 2023. https://doi.org/10.1101/2023.05.09.539985.
14. Duncan Armstrong D. Neuropathology of Rett Syndrome. J Child Neurol. 2005;20:747–53.
15. Kavalali ET, Nelson ED, Monteggia LM. Role of MeCP2, DNA methylation, and HDACs in regulating synapse function. J Neurodev Disord. 2011;3:250–6.
16. Xu X, Kozikowski A, Pozzo-Miller L. A selective histone deacetylase-6 inhibitor improves BDNF trafficking in hippocampal neurons from Mecp2 knockout mice: implications for Rett syndrome. Front Cell Neurosci. 2014;8:68.
17. Duman RS, Aghajanian GK, Sanacora G, Krystal JH. Synaptic plasticity and depression: new insights from stress and rapid-acting antidepressants. Nat Med. 2016;22:238–49.
18. Singleton MK, et al. MeCP2 is required for global heterochromatic and nucleolar changes during activity-dependent neuronal maturation. Neurobiol Dis. 2011;43:190–200.
19. Mellén M, Ayata P, Dewell S, Kriaucionis S, Heintz N. MeCP2 binds to 5hmC enriched within active genes and accessible chromatin in the nervous system. Cell. 2012;151:1417–30.
20. Yang Y, Kucukkal TG, Li J, Alexov E, Cao W. Binding analysis of Methyl-CpG binding domain of MeCP2 and rett syndrome mutations. ACS Chem Biol. 2016;11:2706–15.
21. Sheikh TI, et al. From function to phenotype: impaired DNA binding and clustering correlates with clinical severity in males with missense mutations in MECP2. Sci Rep. 2016;6:38590.
22. Good KV, Vincent JB, Ausió J. MeCP2: the genetic driver of rett syndrome epigenetics. Front Genet. 2021;12:620859.
23. Cuddapah, V. A. et al. Methyl-CpG-binding protein 2 (MECP2) mutation type is associated with disease severity in Rett syndrome. J Med Genet. 2014;51, 152 LP – 158.
24. Lamonica JM, et al. Elevating expression of MeCP2 T158M rescues DNA binding and Rett syndrome-like phenotypes. J Clin Invest. 2017;127:1889–904.
25. Ricceri L, De Filippis B & Laviola G. Rett syndrome treatment in mouse models: Searching for effective targets and strategies. Neuropharmacology. 2013. Preprint at https://doi.org/10.1016/j.neuropharm.2012.08.010.
26. Glaze DG, et al. Double-blind, randomized, placebo-controlled study of trofinetide in pediatric Rett syndrome. Neurology. 2019;92:e1912–25.
27. Butler KV, et al. Rational Design and Simple Chemistry Yield a Superior, Neuroprotective HDAC6 Inhibitor. Tubastatin A J Am Chem Soc. 2010;132:10842–6.
28. Good KV, et al. Trichostatin A decreases MeCP2 expression and phosphorylation levels and increases its chromatin binding affinity. Epigenetics. 2017;12:934–44.
29. Tejido C, Pakravan D, Bosch L. Van, Den. Potential Therapeutic Role of HDAC Inhibitors in FUS-ALS. Front Mol Neurosci. 2021;14:686995.
30. El-Saiy KA, Sayed RH, El-Sahar AE, Kandil EA. Modulation of histone deacetylase, the ubiquitin proteasome system, and autophagy underlies the neuroprotective effects of venlafaxine in a rotenone-induced Parkinson's disease model in rats. Chem Biol Interact. 2022;354:109841.
31. Gadalla KK, et al. Improved survival and reduced phenotypic severity following AAV9/MECP2 gene transfer to neonatal and juvenile male Mecp2 knockout mice. Mol Ther. 2013. https://doi.org/10.1038/mt.2012.200.
32. Van Esch H, et al. Duplication of the MECP2 Region Is a Frequent Cause of Severe Mental Retardation and Progressive Neurological Symptoms in Males. The American Journal of Human Genetics. 2005;77:442–53.
33. Kucukkal TG, Yang Y, Uvarov O, Cao W, Alexov E. Impact of Rett Syndrome Mutations on MeCP2 MBD Stability. Biochemistry. 2015;54:6357–68.
34. Liu M, Landuyt B, Klaassen H, Geldhof P, Luyten W. Screening of a drug repurposing library with a nematode motility assay identifies promising anthelmintic hits against Cooperia oncophora and other ruminant parasites. Vet Parasitol. 2019;265:15–8.
35. Winkler R, et al. Histone Deacetylase 6 (HDAC6) Is an Essential Modifier of Glucocorticoid-Induced Hepatic Gluconeogenesis. Diabetes. 2012;61:513–23.
36. Unterman I, et al. Expanding the MECP2 network using comparative genomics reveals potential therapeutic targets for Rett syndrome. Elife. 2021;10:e67085.
37. Park S-Y, Kim J-S. A short guide to histone deacetylases including recent progress on class II enzymes. Exp Mol Med. 2020;52:204–12.
38. Hassig CA, Fleischer TC, Billin AN, Schreiber SL, Ayer DE. Histone Deacetylase Activity Is Required for Full Transcriptional Repression by mSin3A. Cell. 1997;89:341–7.
39. Nan X, et al. Transcriptional repression by the methyl-CpG-binding protein MeCP2 involves a histone deacetylase complex. Nature. 1998;393:386–9.
40. Eckschlager T, Plch J, Stiborova M, Hrabeta J. Histone Deacetylase Inhibitors as Anticancer Drugs. Int J Mol Sci. 2017;18:1414.

Publisher's Note